USE OF ELECTRON BACK SCATTER DIFFRACTION IN UNDERSTANDING TEXTURE AND THE MECHANISMS OF BACK SCATTERED NOISE GENERATION IN TITANIUM ALLOYS

P. D. Panetta, R. B. Thompson, and F. J. Margetan

Center for NDE, Iowa State University
1915 Scholl Rd.
Ames, IA 50011

INTRODUCTION

Developing a quantitative understanding of ultrasonic beam propagation in engineering materials such as Ti-6Al-4V is important because flaw signals can be altered greatly by the macrostructure that the ultrasonic beam propagates through between the transducer and the flaw. Two consequences of the macrostructure are particularly important: 1) back scattered noise which competes with flaw signals and 2) forward scattered signals and the associated beam profile fluctuations which can modulate the strength of flaw signals [1,2,3]. These effects are particularly important when ultrasonic beams are used to detect subtle defects such as unvoided, uncracked hard-alpha inclusions (regions with a high content of interstitial nitrogen or oxygen), because the flaw signal is inherently weak due to a small mismatch of acoustic impedance. Each of these effects is controlled by the inherently complex macrostructure which develops during routine processing. Current theories suggest that the most important physical feature which controls noise is the two-point correlation of elastic constants, which is in turn controlled by local variations in crystallographic orientation [4]. Therefore, in order to quantify the effects of the macrostructure on ultrasonic beam propagation, one must determine the elastic constants on a microscopic level with length scales less than the ultrasonic wavelength, approximately 600 μm at 10 MHz.

This paper presents a test of these theories. In the following sections we will describe the samples used for this study and their macrostructure, microstructure, and the ultrasonic methods used to characterize the macrostructure. We also will present microtexture results obtained using a new Scanning Electron Microscopy technique which enables the measurement of local crystallite orientations with micrometer or better resolution. The local orientations will be used to determine the two-point correlation of elastic constants, which serves as input into theories of noise generation. After a comparison of theoretical predictions to experiment, conclusions and suggested directions of future work will be presented.

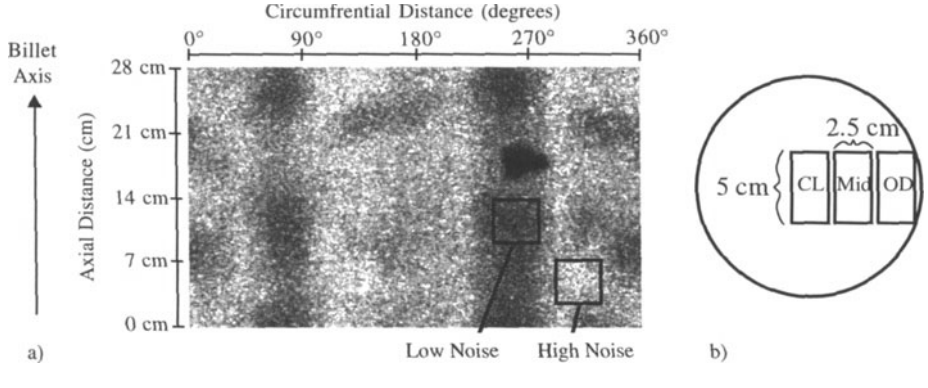

Figure 1. (a) Gated peak-to-peak backscattered noise voltage for radial propagation (4.0 μs time gate centered 2.54 cm deep, focused 3.8 cm deep) and (b) sample location as viewed along the billet axis.

Review of Progress in Quantitative Nondestructive Evaluation, Vol 17
Edited by D.O. Thompson and D.E. Chimenti, Plenum Press, New York, 1998

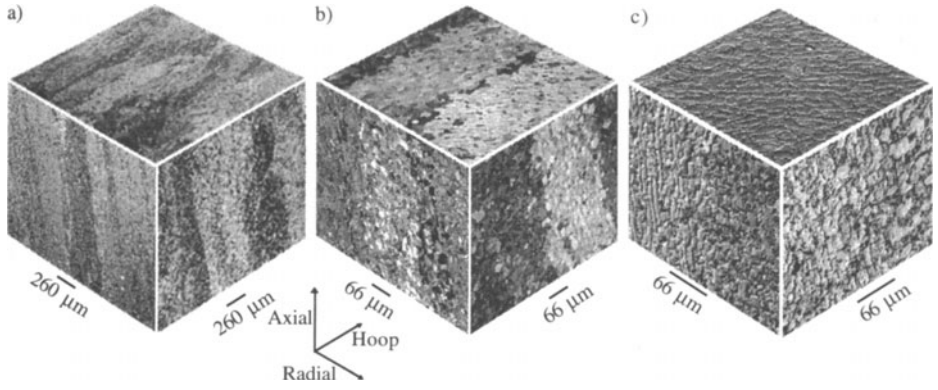

Figure 2. The high noise sample (outside diameter) micrographs, (a) macrostructure, viewed with crossed polarized light, (b) microstructure, viewed with crossed polarized light, and (c) microstructure.

SAMPLES, MACROSTRUCTURE, AND MICROSTRUCTURE

The Ti-6Al-4V samples used for this study were cut from a 15.25 cm (6") diameter billet which exhibited circumferential variations in back scattered noise for radial propagation. Fig. 1a shows a c-scan image of the gated peak-to-peak, backscattered noise voltage where alternating high noise and low noise vertical bands are visible. A high noise region is indicated by a lighter shade and a low noise region by a darker shade. This noise banding is commonly observed in titanium alloy billets and is a result of the complex thermomechanical history. The black triangular shape corresponds to a location where a double layer of duct tape was placed to ensure registry of the image with the billet. It is interesting and important to note that the center of the high noise and low noise regions are separated by ~90°. An interpretation of the consequences of this and a reason for it will be discussed in the next section.

Since inspections for defects are typically performed in the radial direction, this noise can inhibit the detectability of small flaws. There is a great desire to determine the origin of the high noise, low noise banding in order to improve detectability; obviously a uniform low noise level would be preferable. To systematically study the variations in noise that occur in this Ti-6Al-4V billet, samples were cut from the high noise and low noise regions. Three samples measuring approximately, 5 cm x 2.5 cm x 6 cm, were cut from different depths from a high noise region and a low noise region shown in Fig. 1b.

DESCRIPTION OF MACROSTRUCTURE AND MICROSTRUCTURE

Thermomechanical working both above and below the beta transus (~1000°C) produced the complex, duplex structure shown in Fig. 2 and 3 for the high noise and low noise outside diameter samples respec-

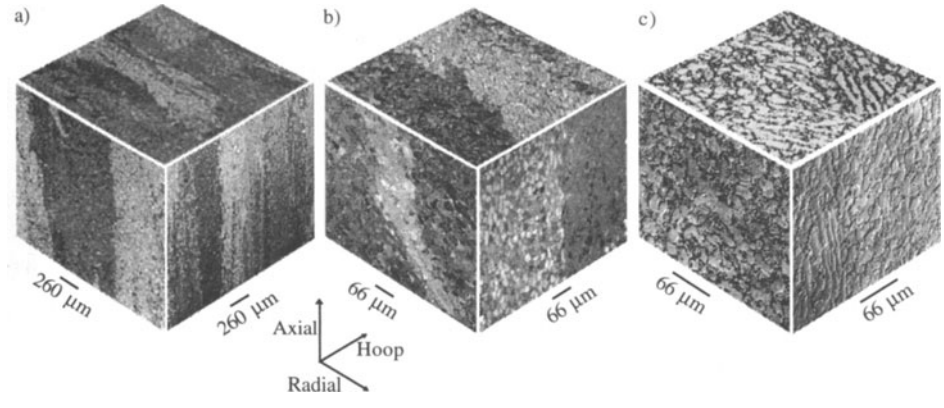

Figure 3. The low noise sample (outside diameter) micrographs, (a) macrostructure, viewed with crossed polarized light, (b) microstructure, viewed with crossed polarized light, and (c) microstructure.

tively. Deformation above the beta transus produced the features which we interpret as elongated beta (BCC) grains on the order of many 1000's of μm's in length and hundreds of μm wide. After a martensitic transformation, these beta grains were converted to many alpha (HCP) grains ranging from 10 μm to 100 μm in size with correlated crystallographic orientations, as seen in Fig. 2c and 3c.

The micrographs in Fig. 2a, 2b, 3a, and 3b were taken with crossed polarized light, and therefore, contrast is due to orientation differences between the alpha crystallites which reflect that of the prior beta grains. Each shaded region has a similar orientation and thus similar elastic constants. In both the high noise and the low noise sample there is elongation of the prior beta grains on the order of a cm in the axial direction, as seen in the micrographs of sections perpendicular to the hoop and radial directions (left and right faces of Fig. 2a and 3a). We therefore, expect low noise for propagation in the axial direction because the macrograins offer a relatively small cross section, as compared with radial or hoop propagation. Interestingly, and related to the complex processing of this particular billet, is the fact that there is also elongation in the hoop direction in the high noise sample (top face of Fig. 2a and 2b), while in the low noise sample there is elongation in the radial direction as seen in the micrographs of sections perpendicular to the axial direction (top face of Fig. 3a and 3b). This secondary elongation of prior beta grains likely occurred as the billet was rolled from a square cross-section to a rectangular cross-section above the beta transus. This operation is atypical for titanium billets used for rotating aircraft engine components. Thus in addition to elongation of prior beta grains in the axial direction we observe secondary elongation to a lesser degree in the hoop direction in the high noise sample and the radial direction in the low noise sample. Considering that the center of the high noise and low noise regions are separated by ~90° , this is not surprising, indicating that the secondary elongated macrograins are possibly parallel to the long axis of the rectangular cross-section produced after rolling, and are visible in the high noise and low noise samples (Fig. 2a and 3a) extracted, even though, they came from region which were separated by ~30°. Physically the secondary elongation could account for the noise banding because the prior beta grains present a larger cross-section for radial propagation in the high noise sample and hence create a higher noise relative to the low noise sample. In addition, we can expect anisotropic noise for hoop and radial propagation. There is little or no difference in the microstructure between the high noise and the low noise samples as can be seen in Fig. 2c and 3c, where the micrographs were taken employing a Normarski differential interference contrast method where contrast is enhanced due to surface relief. In addition the scale of the digital images have been inverted to enhance visibility upon printing. These operations were necessary to achieve a distinct view of the individual grains for the light Kroll's etch performed. The thermomechanical history produced complex microstructures where, in any given region, there is a mix of elongated grains and equiaxed grains. Because the length scale of the microstructure (on the order of tens of μm's) is much less than the ultrasonic wavelength, (600 μm at 10 MHz) it is reasonable to conclude that the microstructure does not dominate to noise generation and it is the macrostructure which controls the noise generation in this duplex titanium alloy [4]. The series of micrographs shown in Fig. 2 and 3 reveals the duplex character of these alloys. There is long range correlation of orientation over millimeters or more, within a given prior beta grain, which is composed of individual alpha grains with length scales less than 100 μm's. The physical picture based on cross-sectional areas of macrograins, leads to a successful qualitative description of the noise. Models and Scanning Electron Microscopy work allow for a quantitative description, as will be discussed subsequently.

ULTRASONIC EXPERIMENTAL MEASUREMENTS

In order to ultrasonically probe the texture variations between the high noise and low noise regions we measured both longitudinal wave (L-wave) and shear wave (S-wave) velocity for axial, radial, and hoop propagation. To probe the scattering variations we measured the back scattered noise, and attenuation in the high noise and low noise regions for axial, radial, and hoop propagation. Velocity measurements were performed on the samples taken from the outside diameter, mid line, and center line of the billet in both the high noise and low noise regions. Noise and attenuation measurements were only measured for the outside diameter samples at this time. In succeeding sections we will describe the velocity measurements, followed by the noise and attenuation measurements.

Velocity Measurements

Velocity measurements were performed to probe the elastic anisotropy, an indication of texture (preferred orientation). The primary motivation was to establish texture, and the texture differences between the high noise and the low noise regions, which developed in this Ti-6Al-4V alloy due to thermomechanical processing.

Longitudinal and shear wave velocities were calculated by measuring the arrival times of the first few back-surface (BS) echoes for waves launched on three orthogonal faces of the samples, (propagating in the axial, radial, and hoop directions). The velocity was determined by the standard procedure in which the waveforms of subsequent echoes were overlapped. S-wave measurements were made with a 1.27 cm (½") diameter contact transducer having a nominal center frequency of 5 MHz, and excited with a broadband pulse. Both polarizations for each propagation direction were examined. The L-wave velocity measurements were performed in water immersion with a 1.27 cm (½") diameter transducer having a nominal center frequency of 10 MHz excited with a broadband pulse. For each propagation direction, measurements were made at three different sites and their average was used for the subsequent calculations.

Noise Measurements

Ultrasonic backscattered noise was measured to determine the degree of its anisotropy and to study the noise generating characteristics of the macrostructure in the high noise and low noise regions. Details of the experimental procedure were given previously, [5] therefore, only a brief outline of the portion of the experimental setup relevant to this work will be given here. Noise measurements were made using a 1.27 cm (½") diameter, 15 MHz transducer with a nominal focal length of 23.7 cm (9.35") excited with a broadband pulse and scanned above one surface of the sample at normal incidence. To ensure good statistics, back scattered noise RF waveforms were collected at 100 or more locations, with care taken to ensure that the beam did not interact with the sides of the sample. Noise waveforms were collected in the time region between the front surface and the back surface echoes and analyzed within a 2.56 μs time gate centered in the focal zone of the beam 1.5 cm deep. The influence of the measurement system was removed by the use of a back surface reference echo from fused quartz, resulting in the determination of the noise Figure of Merit (FOM) as a function of frequency. The FOM is a measure of the noise generating capacity of the microstructure, and is equal to the square root of the backscattering coefficient.

Attenuation Measurements

To further probe scattering in the high noise and low noise regions, attenuation was inferred using a traditional, pulse-echo technique (P/E). The details of the experimental setups may be found in reference [1], and therefore, only a brief overview will be given here. Attenuation was determined from the amplitude of a BS echo of the Ti-6Al-4V sample observed in a P/E setup, as compared to a BS echo in a fused quartz specimen. The measurements were made with a 1.27 cm (½") diameter planar transducer with a center frequency of 10 MHz, excited with a broadband pulse. Multiple attenuation measurements were made in Ti-6Al-4V by scanning the transducer above the surface of the sample at a fixed water path of 2 cm. At each location, an FFT was performed on the received BS echo, and compared to the FFT of the fused quartz reference echo. The attenuation as a function of frequency, $\alpha(f)$, was calculated at each location using Eqn. 1 and averaged over all transducer positions, where $\Gamma(f)$ is the Fourier spectra of the measured voltage. The attenuation of fused quartz was assumed to be negligible.

$$|\Gamma(f)| = |\beta(f)T_{01}R_{10}T_{10}D(f)|\, e^{-2\alpha(f)z} \qquad (1)$$

T and R are the plane-wave transmission and reflection coefficients with "0" designating water and "1" designating Ti-6Al-4V. D(f) is the Lommel diffraction correction [6], $\alpha(f)$ is the attenuation coefficient, and z is the thickness of the Ti-6Al-4V sample. By comparison with the BS echo from fused quartz, whose strength is governed by a similar equation, the transducer efficiency factor, $\beta(f)$, was eliminated and the attenuation of Ti-6Al-4V was deduced. Such a measurement of attenuation has contributions from both energy loss (back scattering) and beam distortion (forward scattering) [1,2,3].

MICROTEXTURE DETERMINATION

In addition to the macroscopic or average texture information gained from the velocity measurements, we studied the local texture variations (microtexture). Samples for microtexture measurements were cut from the ultrasonically scanned regions and the microtexture data was collected in the region of the focal zone of the transducer where noise was calculated to ensure that the microtexture information and ultrasonic data were influenced by the same macrostructure and microstructure. The samples were polished and etched using standard metallographic preparations. Analysis was conducted using a new measurement technique supplied commercially by Tex SEM Laboratories, Inc. termed OIM™. To obtain a measurement of the local orientation as a function of position, this technique analyzes the Kikuchi patterns generated by the back scattered electrons of the electron beam of a Scanning Electron Microscope (SEM) as the electrons diffract from the lattice. Because of the inherently small size of the SEM beam (~nm), OIM™

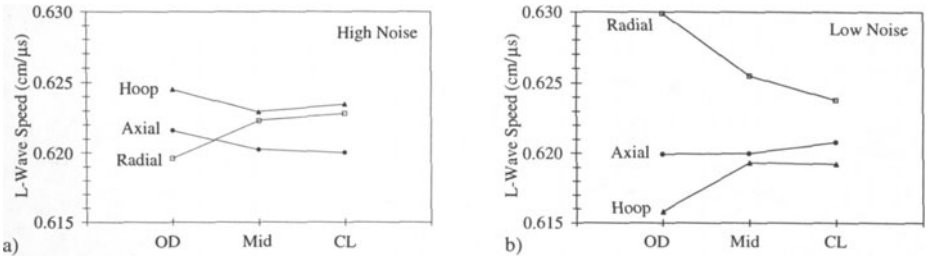

Figure 4. L-wave velocity for hoop, axial, and radial propagation as a function of depth for (a) the high noise region and (b) the low noise region.

allowed the determination of texture information with a fine resolution on small areas in the microstructure. One output of the software is the Euler angles defining crystallite orientation as a function of position. Elastic constants as a function of position were calculated by performing rotations of the polycrystalline elastic constants of Ti-6Al-4V by the calculated Euler angles. The two point correlation of elastic constants <C(r)C(r')> was then calculated. Here C(r) is a component of the elastic stiffness tensor, r and r' are positions of points randomly selected, and <...> denotes an ensemble average. The direct calculation of the <C(r)C(r')> was input into the back scattered grain noise model developed by Han et al. [4] and allowed the theoretical prediction of grain noise and validation of the assumption that the back scattered grain noise is controlled by <C(r)C(r')>, as will be shown in a later section. Another feature of the software is the ability to calculate pole figures, which we used to study the microtexture that developed in the billet due to thermomechanical treatment.

VELOCITY RESULTS

Results for L-wave velocity for the outside diameter, (OD), midline (Mid), and center line (CL) samples are shown in Fig. 4. The velocity for the high noise and the low noise sample are plotted vs. depth. It is important to note that the velocity is anisotropic with the largest anisotropy on the outside of the billet. Furthermore, the anisotropy diminishes as we move towards the center of the billet for both the high noise and the low noise regions, with the fastest velocity for hoop propagation in the high noise region while for the low noise sample the fastest velocity is for radial propagation. The diminution of anisotropy is most pronounced in the low noise region. Closer inspection of velocity in the high noise sample indicates the highest velocity is in the hoop direction with radial being lowest and axial being intermediate. While in the low noise region radial propagation is fastest and hoop slowest with axial again being intermediate. The anisotropy in velocity and differences between the high noise and low noise regions indicates qualitatively that the thermomechanical deformation produced different texture in the high noise and low noise regions and texturing diminished with depth. Because the velocity of a Ti-6Al-4V alpha (HCP) phase single crystal is anisotropic, with propagation along the c-axis fastest, the data implies that the c-axis tends to point in the hoop direction in the high noise region and in the radial direction in the low noise region parallel to the secondary elongation. We will show microtexture data in a subsequent section that is in agreement.

To quantify the degree and type of texture differences between the high noise and the low noise regions we calculate the texture parameters referred to as orientation distribution coefficients (ODC'S) using the equations from reference [7,8]. Results of the differences between the ODC's in high and low noise regions are shown in Table I. For the coordinate system chosen, W_{400} is largest when the c-axis is aligned with the radial direction of the billet. Thus the results quantify the fact that the low noise samples have a greater fraction of the basal poles oriented along the radial direction and that the differences are most pronounced on the outside of the billet.

Table I. Orientation distribution coefficients, W_{200} and W_{400}, for the high noise (HN) and low noise (LN) regions. The difference of W_{lmn} between the HN and LN regions are presented where positve difference indicates a higher probability of the c-axis to be aligned with the radial direction of the billet for the LN sample.

OD	W_{200}	W_{400}
LN - HN	0.0167	0.0121

Mid	W_{200}	W_{400}
LN - HN	0.0054	0.0051

CL	W_{200}	W_{400}
LN - HN	0.0038	-0.0050

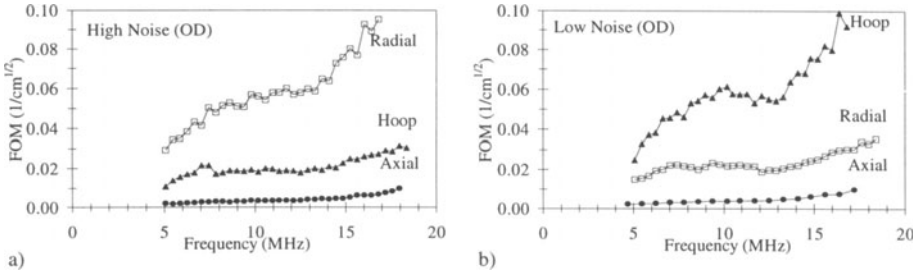

Figure 5. FOM as a function of frequency for (a) the high noise sample (outside diameter) and (b) the low noise sample (outside diameter).

NOISE RESULTS

The noise FOM as a function of frequency is plotted for the high noise and low noise samples in Fig. 5a and b respectively for the outside diameter sample. Most notable is the anisotropic nature of the noise in both samples. For the high noise sample, radial propagation produces the highest noise, axial propagation the lowest noise and hoop propagation produces intermediate values. This anisotropy in noise can be understood physically because the macrograins are primarily elongated in the axial direction and hence present the smallest cross section and thus lower noise for axial propagation. The additional anisotropy in the noise for the high noise sample between the hoop and radial direction can be related to the different degrees of elongation in the hoop and radial directions, as was shown in Fig. 2a and discussed in the accompanying text. In the low noise sample we see noise anisotropy as well but with the ordering for hoop propagation and radial propagation reversed, with hoop propagation producing the largest FOM. The noise anisotropy agrees with the idea that the larger the cross section of the macrograin presented to the ultrasonic beam the larger the noise.

ATTENUATION RESULTS

Attenuation data shows similarly strong anisotropy, where attenuation as a function of frequency is shown in Fig. 6a and 6b for the high noise sample and low noise sample respectively. However, propagation directions producing high noise produce low attenuation and propagation directions producing low noise produce high attenuation. These results indicate that noise and attenuation are intimately related, implying the two properties are governed by the same scattering phenomena. Physically the attenuation anisotropy can be due to the wavefront of the beam becoming distorted as it propagates through the sample, artificially decreasing the voltage received from a piezoelectric transducer, with propagation parallel to the elongated macrograins producing the largest degree of distortion and thus the highest attenuation [1]. Existing theories for noise use the Born approximation which is inadequate to describe the multiple forward scattering which controls attenuation [9]. Very recent theoretical results predicting attenuation in FCC aluminum with elongated grains show an increase in attenuation for propagation directions parallel to grain elongation, consistent with our observations in titanium alloys [10].

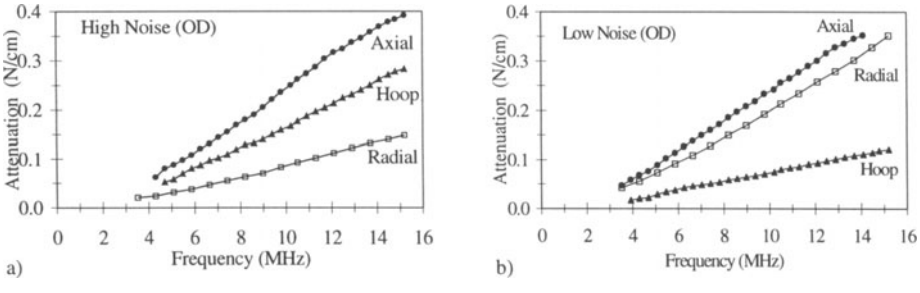

Figure 6. Attenuation as a function of frequency for (a) the high noise sample (outside diameter) and (b) the low noise sample (outside diameter).

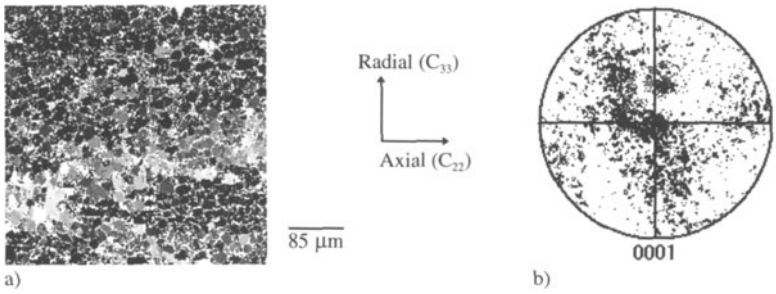

Figure 7. Microtexture results for high noise sample (outside diameter) hoop face: (a) C-scan of C_{22} (425 μm x 425 μm, 2 μm step) and (b) 0001 pole figure.

MICROTEXTURE RESULTS

Previous work suggests that noise and attenuation are controlled by the two point correlation of elastic constants [4]. In the past, this has been estimated by measuring an average grain size and assuming that the two point correlation of elastic constants is an exponentially decaying function of distance between points. While this is reasonable for microstructures with uncorrelated orientations, it can grossly underestimate the two point correlation of elastic constants that occurs for the elongated macrostructure typically seen in these Ti-6Al-4V billets, as shown in Fig. 2a and 3a. Recently a superior method that enables direct determination of the two point correlation of elastic constants was developed by Wright et al. [11] and commercialized by Tex SEM Labs. By performing rotations of the polycrystalline elastic constants of Ti-6Al-4V by the calculated Euler angles, the elastic constants as a function of position were mapped on the three orthogonal faces defined in Fig. 2 and 3, and the two point correlation of elastic constants was input into the following equation to calculate FOM, developed by Han et al. [4], for comparison with experimental measurements. In the analysis here, $\delta\rho$ is assumed to be zero, a simplification of Eqn. 6 in reference 4.

$$FOM^2 = \frac{k^4}{(4\pi\rho V_l^2)^2}\int d^3\mathbf{r} <\delta C_{33}(\mathbf{r})\delta C_{33}(\mathbf{r}')> e^{2ikz} \qquad (2)$$

Typical results from the SEM scan for the high noise sample are shown in Fig. 7, where the c-scan of C_{22} is shown, which controls the backscattered noise for longitudinal waves propagating in the axial direction. There is a band of common elastic constants (light shade) in the center of the scanned region, elongated in the axial direction (horizontal), indicating a common orientation in this region. The 0001 pole figure from this 425 μm x 425 μm region is shown in Fig. 7b where we can see strong microtextureing with the c-axis aligned with the hoop direction (out of the paper), as indicated by a higher density of points in the center. For comparison with the high noise sample, a c-scan of C_{22} for the low noise sample is shown in Fig. 8a and we again see a band elongated along the axial direction (horizontal) for this 250 μm x 800 μm scan region. From the pole figure in Fig. 8b and we can see the c-axis tends to be aligned between the radial and hoop direction with a strong component in the radial direction in contrast with high noise sample. This preferred orientation indicates that there are microtexture differences between the high noise and low noise regions in agreement with the macrotexture information from the velocity data, with the c-axis parallel to the secondary elongation of the macrograins.

By calculating the two point correlation of C_{11}, C_{22}, and C_{33} on three orthogonal faces the noise FOM can be calculated using equation 2. To appropriately perform the integrals in equation 2, $<C_{II}(r)C_{II}(r')>$, where I =1,2, and 3, was calculated in two orthogonal directions on each face. The

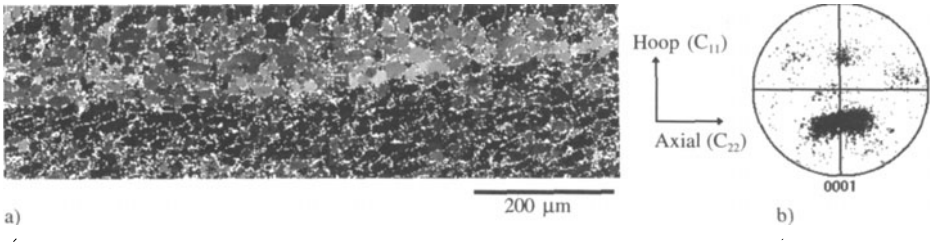

Figure 8. Microtexture results for low noise sample (outside diameter), radial face, (a) C-scan of C_{22} (250 μm x 800 μm, 2 μm step) and (b) 0001 pole figure.

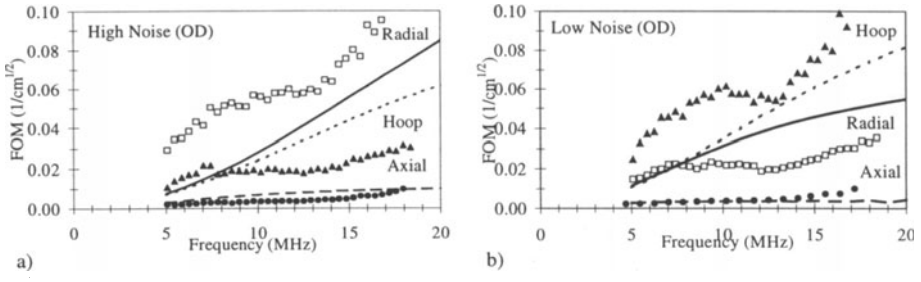

Figure 9. Experimental(points) and theoretical (lines) FOM as a function of frequency for (a) the high noise sample (outside diameter), and (b) the low noise sample (outside diameter). Radial propagation (unfilled squares and solid line), hoop propagation (filled triangles and dotted line), and axial propagation (filled circles and dashed line).

integration was performed numerically using Simpson's rule. Details of the assumptions and calculations will be presented in a future publication. Both the experimental FOM (solid points) and theoretical FOM (lines) are plotted assuming no attenuation in Fig. 9a and b for the high noise sample and low noise sample respectively. Numerical agreement is seen to be good and the anisotropy of FOM in the high noise and low noise samples is accurately predicted. It is our belief that this is the first report of noise FOM prediction from a direct measurement of the two point correlation of elastic constants. The good agreement between theory and experiment, both in terms of absolute value and anisotropy, independently confirms that the two point correlation of elastic constants controls ultrasonic noise generation.

CONCLUSIONS AND FUTURE WORK

This work produced two important results: 1) we quantified the texture and ultrasonic scattering variations between the high and low noise regions that occurred due to the thermomechanical processing of a particular titanium billet and 2) we successfully predicted the observed noise anisotropy based on an existing theory and a direct measurement of the two point correlation of elastic constants. In addition, we observed variations in macrostructure, texture and ultrasonic scattering in both the circumferential and radial directions showing the correlation between the macrostructure and ultrasonic properties.

Directions for future work include ultrasonic noise and attenuation measurements on samples deeper in the billet, as well as further microtexture measurements. In addition, we will compare microtexture results with macrotexture results obtained using x-rays. Furthermore, work is currently being performed to develop a model of attenuation in these highly anisotropic, duplex titanium alloys.

ACKNOWLEDGMENTS

The authors would like to thank Fran Laabs of Ames Laboratory for his tireless SEM work. This work was supported by the Engine Titanium Consortium under the Federal Aviation Administration Grant No. 94-G-048.

REFERENCES

1. P. D.Panetta, F. J. Margetan, I. Yalda, and R. B. Thompson, Review of Progress in QNDE, Vol.15B (1996) pp 1525-32.
2. P. D.Panetta, F. J. Margetan, I. Yalda, and R. B. Thompson, Review of Progress in QNDE, Vol.16B (1997) pp 1547.
3. F. J. Margetan, P. D. Panetta, and R. B. Thompson, Review of Progress in QNDE, These Proceedings.
4. Y. K. Han and R. B. Thompson, Metallurgical and Materials Transactions A, Vol. 28A (1997) pp 91-104.
5. F.J.Margetan, T.A.Gray, and R.B.Thompson, Review of Progress in QNDE, Vol. 10B (1991) pp 1721-28.
6. P. H. Rodgers and A. L. Van Buren, J. Acoust. Soc. Am. Vol. 55 (1974). pp 724-28.
7. Y. K Han, R. B. Thompson, A. J. Anderson, M. Hirao, and J. Root, (Manuscript).
8. Yan Li and R. Bruce Thompson, J. Appl. Phys. Vol. 67 (5) (1990) pp 2663-65.
9. P. D. Panetta, R. B. Thompson, F. J. Margetan, and I. Yalda, NDE and Material Properties III, The Minerals, Metals, & Materials Society, (1997) pp 9-16.
10. S. Ahmed and R. B. Thompson, Review of Progress in QNDE, These Proceedings.
11. Stuart I. Wright and Brent L. Adams, Metallurgical Transactions A, Vol. 23A (1992) pp 759-67.